

Ion mobility measurements in Ar-CO₂, Ne-CO₂, and Ne-CO₂-N₂ mixtures, and the effect of water contents

Alexander Deisting^{a,b,*}, Chilo Garabatos^a, Alexander Szabo^c

^aGSI Helmholtzzentrum für Schwerionenforschung GmbH, Planckstraße 1, Darmstadt, Germany

^bPhysikalisches Institut, Ruprecht-Karls-Universität Heidelberg, Heidelberg, Germany

^cFaculty of Mathematics, Physics and Informatics, Comenius University, Bratislava, Slovakia

Abstract

A detector has been constructed for measuring ion mobilities of gas mixtures at atmospheric pressure and room temperature. The detector consists of a standard triple GEM amplification region and a drift region where ions drift. A method has been developed to measure the ions' arrival time at a cathode wire-grid by differentiating the recorded signals on this electrode. Simulations prove that this method is accurate and robust. The ion mobility in different gas mixtures is measured while applying different drift field values ranging from 200 V cm⁻¹ to 1100 V cm⁻¹.

From an extrapolation of a Blanc's law fit to measurements in Ar-CO₂ mixtures we find the reduced mobility of the drifting (cluster) ion species in pure argon to be 1.94 ± 0.01 cm² V⁻¹ s⁻¹ and in pure carbon-dioxide to be 1.10 ± 0.01 cm² V⁻¹ s⁻¹. Applying the same procedure to our measurements in Ne-CO₂ yields 4.06 ± 0.07 cm² V⁻¹ s⁻¹ and 1.09 ± 0.01 cm² V⁻¹ s⁻¹ for the reduced mobilities in pure neon and carbon-dioxide, respectively.

Admixtures of N₂ to Ne-CO₂ (90-10) reduce somewhat the mobility. For the baseline gas mixture of the future ALICE Time Projection Chamber, Ne-CO₂-N₂ (90-10-5), the measured reduced mobility of the drifting ions is 2.92 ± 0.04 cm² V⁻¹ s⁻¹.

Ion mobilities are examined for different water content ranging from 70 ppm to about 2000 ppm in the gas using Ar-CO₂ (90-10) and Ne-CO₂ (90-10). A slight decrease of ion mobility is observed for the addition of several hundred ppm of water.

Keywords: Ion mobility, Gaseous detectors, ALICE time projection chamber

1. Introduction

The ion mobility (K) is the factor relating the drift velocity (v_{Drift}) of ions to the drift field (E_{Drift}): $v_{\text{Drift}} = K \cdot E_{\text{Drift}}$ [1]. Under high particle loads, *i.e.* on the order of several nA cm⁻² reaching the readout plane, ions can accumulate in the drift volume of a gaseous detector. These ions produce a large space charge distorting the drift field. Such distortions and their possible mitigation have been and are studied by many experiments as *e.g.* the current ALICE Time Projection Chamber [2] (TPC) [3], the upgraded ALICE TPC [4, 5] and the LCTPC [6, 7]. If K is known, it is possible to estimate and simulate this space charge and to evaluate the impact of the back drifting ions on the performance of a detector.

Mobilities of ions in their parent gases (*e.g.* Ne⁺ in neon) have been measured extensively, *cf.* [8, 9, 10, 11], but the mobility of an ion species in a gas mixture differs from its mobility in the parent gas. With this study we provide ion mobilities for different gas mixtures commonly used in gaseous detectors and in particular we measure the mobility in the gas mixture of the upgraded ALICE TPC, Ne-CO₂-N₂ (90-10-5) [5].

To measure the ion drift velocity a dedicated set-up is constructed, which is described in Section 2. The principle of the

measurements and the signal analysis procedure follow in Section 3. In Section 3.1 we describe our method to determine the ions' time of arrival at the end of the drift gap and we demonstrate with simulations that the method is accurate and robust. Afterwards the measurement of the signal indicating that the ions started to drift (Sec. 3.4) and the different uncertainties affecting the mobility measurements (Sec. 4.1) are discussed. The ion mobility found for different Ar-CO₂ and Ne-CO₂ gas mixtures are presented as a function of E_{Drift} (Sec. 4.2) and as function of the quencher content in the gas mixture (Sec. 4.3). Furthermore the effect of admixtures of N₂ to Ne-CO₂ (90-10) is examined (Sec. 4.4) and the effect of water on the ion mobility is studied using Ar-CO₂ (90-10) and Ne-CO₂ (90-10) (Sec. 4.5). We summarise our findings in Section 5.

2. Experimental set-up

The experimental set-up is described in [12], nevertheless we give a short summary. We use a detector (Fig. 1) with a triple Gas Electron Multiplier (GEM) [13] stack with standard 10 × 10 cm² foils. The transfer gaps 1 and 2, and the induction gap have a width of 2 mm. Above the GEM stack a wire-grid (wire spacing/diameter: 2 mm/100 μm) is mounted at a distance of $d_{\text{Drift}} = 21.35 \pm 0.12$ mm. The grid is followed at a distance of $d_{\text{T3}} = 6.4 \pm 0.2$ mm by a mesh serving as drift cathode. This

*Corresponding author

Email address: alexander.deisting@cern.ch (Alexander Deisting)

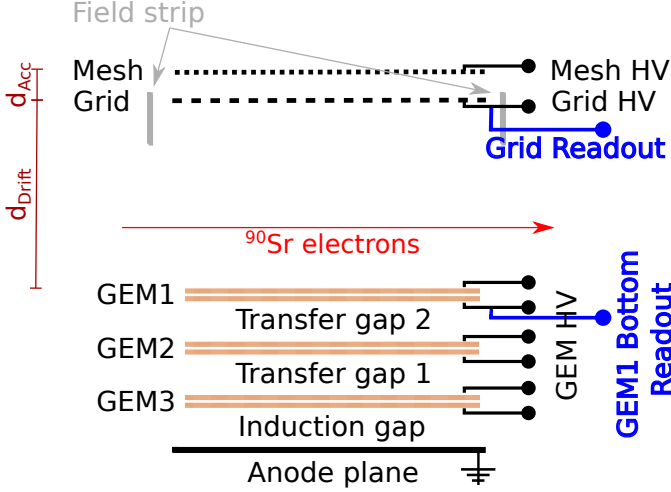


Figure 1: Set-up for the measurement of ion mobility. Signals from the GEM1 bottom electrode and the wire-grid are passed on to a preamplifier and to a digital oscilloscope where individual signals are stored for later processing or several signals are averaged and then the average is stored.

region between grid and mesh (GEM1 top, respectively) is referred as *transfer gap 3* (*drift gap*, respectively). A field strip mounted at the GEM-stack-side of the grid is used to improve the field homogeneity.

We use an open gas system employing Bronkhorst F-201CV [14] mass flow controllers which allow one to mix up to three different gases. The detector exhaust consist of several metres of 4 mm pipe. The temperature is monitored by the lab's air conditioning system and the atmospheric pressure is recorded by a transmitter of the CTE7000 series [15] located elsewhere. Both values are used to correct the measured mobilities. A DewMaster water sensor [16] is placed shortly after the detector in the gas exhaust line, to monitor the water content of the counting gas. The sensor is a double-cooling stage chilled mirror hygrometer with a precision of 1 ppm.

Each electrode is powered with an individual channel of either a CAEN N471 [17] Power Supply (PS) or a CAEN N470 [18] PS, therefore, the voltage on each electrode can be tuned individually.

Signals are decoupled from the High Voltage (HV) line to the wire-grid using a $C_{Dec} = 20$ nF capacitor and afterwards the signals are fed into an ORTEC 142IH [19] preamplifier. A similar preamplifier is used to decouple and process the signals from the HV line supplying the GEM1 bottom electrode. This preamplifier is suitable for millisecond rise time signals, as confirmed with a pulse generator.

3. Principle of measurement

Electrons from primary tracks in the drift gap drift to the GEM stack. The ions from the gas amplification produced in GEM3 and GEM2 drift through the stack and induce a signal on the GEM1 bottom electrode, as they leave the GEM stack at a time t_{GEM} . Afterwards the ions drift in a uniform electric field towards the wire-grid. Behind the grid a similar field as in the drift gap is set. Throughout the entire time of ions moving

in the drift gap and in the transfer gap 3, a signal is induced on the grid. The time at which the ions cross the grid (t_{Grid}) is extracted from this signal (Sec. 3.1). We use the time difference $t_{Drift} = t_{Grid} - t_{GEM}$ and the known length of the drift gap to calculate the ions velocity $v_{Drift} = \frac{d_{Drift}}{t_{Drift}}$. Then the ion mobility is calculated from this velocity and the voltage difference across the drift gap $\Delta U_{Drift} = U_{GEM1\ Top} - U_{Grid}$

$$K = \frac{v_{Drift}}{E_{Drift}} = \frac{v_{Drift} \cdot d_{Drift}}{\Delta U_{Drift}} = \frac{(d_{Drift})^2}{t_{Drift} \cdot \Delta U_{Drift}} \quad (1)$$

Because the signals are affected by a regular noise in the form of oscillations in the frequency range between about 40 kHz to about 200 kHz (e.g. Fig. 2a), an average of 2000 subsequent signals is used for the data analysis. The average signal is transformed, through fast Fourier transform, into the frequency domain, where frequencies above $f_{Cut} = 10$ kHz are cut out and then the signals are transformed back. Figure 2 illustrates the difference between an individual signal (Fig. 2a), the average over 2000 signals (Fig. 2b) and the corresponding signals after the frequency cut has been applied.

3.1. Measurement of the ion arrival at the grid

At the time the ions pass through the grid, the polarity of the induced signal changes [20]. In the two plots in Figure 2 this is visible in the *Grid signal*.¹ The *Differentiated grid signal* in Figure 2b has distinct peaks, which allow to identify the inflection points. The last inflection point corresponds to the time when ions cross the wire-grid, i.e. t_{Grid} , if the electric fields in the drift gap and transfer gap 3 are the same. Simulations explained below show the robustness of this method.

A configuration with a wire-grid and an homogeneous electric field E_{Drift} (E_{T3} , respectively) in the drift gap (transfer gap 3, respectively) is used to generate signals with Garfield [21] as ions drift and cross the grid. An arbitrary ion mobility is introduced into the simulations and 10^5 ions are initially distributed such that they cover several wire pitches. In drift direction the ion distribution has a Gaussian shape. The drifting ions' signal on the wire-grid is shown in Figure 3 for ions drifting first through the drift gap and then through the transfer gap 3. When the ions approach the grid the signal rises and it becomes more negative after the ions crossed the grid. Eventually the signal is zero, when the ions reach the cathode. Knowledge of E_{Drift} , the inserted ion mobility and the drift distance yields the expected time of arrival at the grid, $t_{Grid}^{Expected}$. However, the signal shape lacks a distinctive feature, which is suitable to measure the time when ions pass through the grid.

Figure 3 shows as well the signals' derivative. There is an inflection point during the period when the signal becomes more negative, which is visible as a peak. This inflection point occurs at $t_{Grid}^{Expected}$, if $E_{T3} = E_{Drift}$. Therefore the inflection point in the ion signal on the wire-grid is suitable to determine t_{Grid} , if the electric field on both sides of the grid is the same.

In order to test the reliability of this inflection point method the simulations are tuned to reproduce the shape of measured signals including the overlaying of a periodic noise (Fig. 4a).

¹The preamplifiers invert the actual signals.

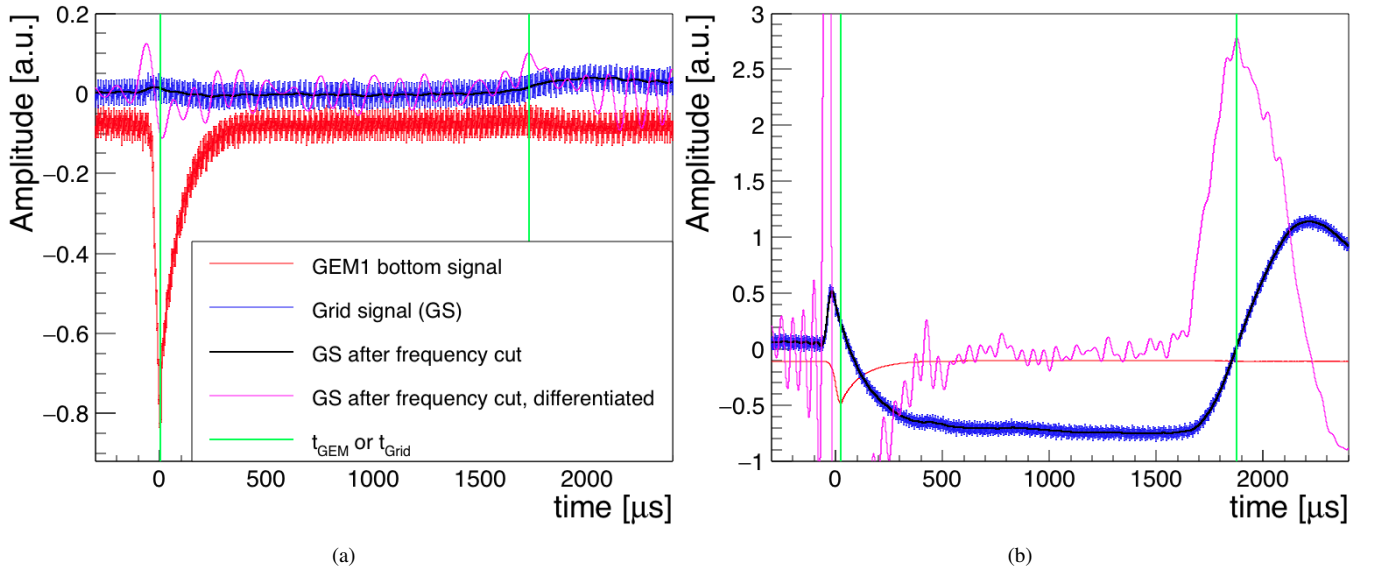


Figure 2: (a) A simultaneous measurement of the signal from the bottom side of GEM1 and the wire-grid and (b) the average of 2000 of such measurements. The legend in Figure (a) applies to both plots. In (b) the *Grid signal* is scaled up by a factor 100 and is shifted at the vertical axis, to fit the scaled signal again into the plot. All measurements are done in Ne-CO₂ (90-10), but the arrival times differ because the gas pressure and temperature in (a) and (b) differ.

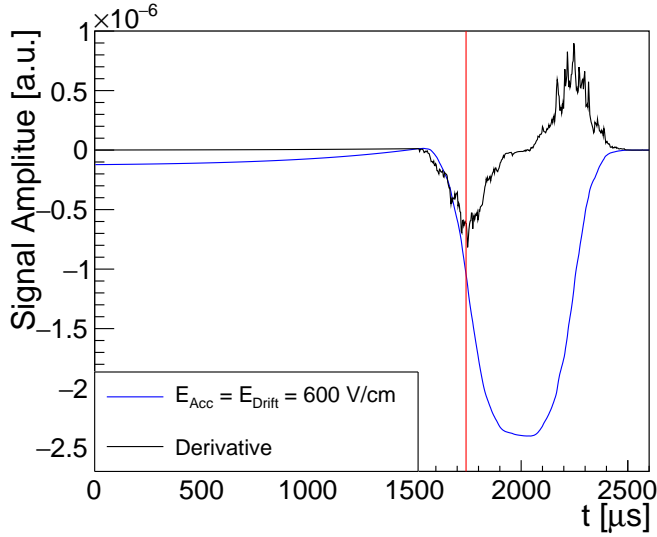


Figure 3: Garfield simulation of the induced ion signal on a wire-grid and its derivative. The vertical red line marks the time at which the ions are expected to arrive at the grid ($t_{\text{Grid}}^{\text{Expected}}$).

The resulting waveforms are then fed in the data analysis chain and the ratio of $t_{\text{Grid}}^{\text{Expected}}$ to t_{Grid} is determined. This is done for different mobilities, varying E_{Drift} and E_{T3} , and different initial ion distributions. For each simulation several values of f_{Cut} are used during the analysis. The range of electric fields in the simulation is similar to the actual fields used during the measurements. Furthermore, the pressure (temperature) in the simulation is set to atmospheric pressure (room temperature) and varied in order to cover the gas conditions during our measurements. The results in Figure 4b illustrates that the inflection point of the grid signal is indeed a reliable measure to determine

t_{Grid} if $E_{\text{Drift}} = E_{\text{T3}}$. The additional ion distributions in the figure include square, triangular, and asymmetric multiple-Gaussian distributions. Figure 4b shows that the results for $t_{\text{Grid}}^{\text{Expected}}/t_{\text{Grid}}$ do not depend on the initial ion distribution in the simulation as long as the drift distance is measured from the centre of gravity of the ion distribution to the grid.

3.2. Discrimination between ions with different mobilities

Simulations similar to the ones presented in Figure 4 are used to examine the case where several ion species with different mobilities drift. The induced signals on the wire grid is simulated in a first step for the respective single ion species. Afterwards, these signals are overlaid to yield one signal of several ions with different mobility. Proceeding in steps is necessary, because Garfield does not offer the possibility to introduce more than one ion mobility. If the arrival time of two ion species differs by more than $\Delta t_{\text{Grid}} = 100 \mu\text{s}$, distinct inflection points are obtained for each species. Using Equation (1), Δt_{Grid} can be translated to a relative difference between two mobilities, which can be resolved by our method:

$$\frac{\Delta K}{K} = \frac{\Delta t_{\text{Grid}} \cdot E_{\text{Drift}}}{d_{\text{Drift}}} \cdot K, \quad ,$$

e.g. for $d_{\text{Drift}} = 21.53 \text{ mm}$, $E_{\text{Drift}} = 400 \text{ V cm}^{-1}$, and $K = 2 \text{ cm}^2 \text{ V}^{-1} \text{ s}^{-1}$ $\Delta K/K$ is 3.7 %.

3.3. Ion signal at the GEM1 bottom electrode

In the simulations discussed in Section 3.1 the initial ion distribution is an input to the calculations, so its centre of gravity is known as is the start-time t_{GEM} of the ion mobility measurement. In the real set-up the ion distribution is a result of the

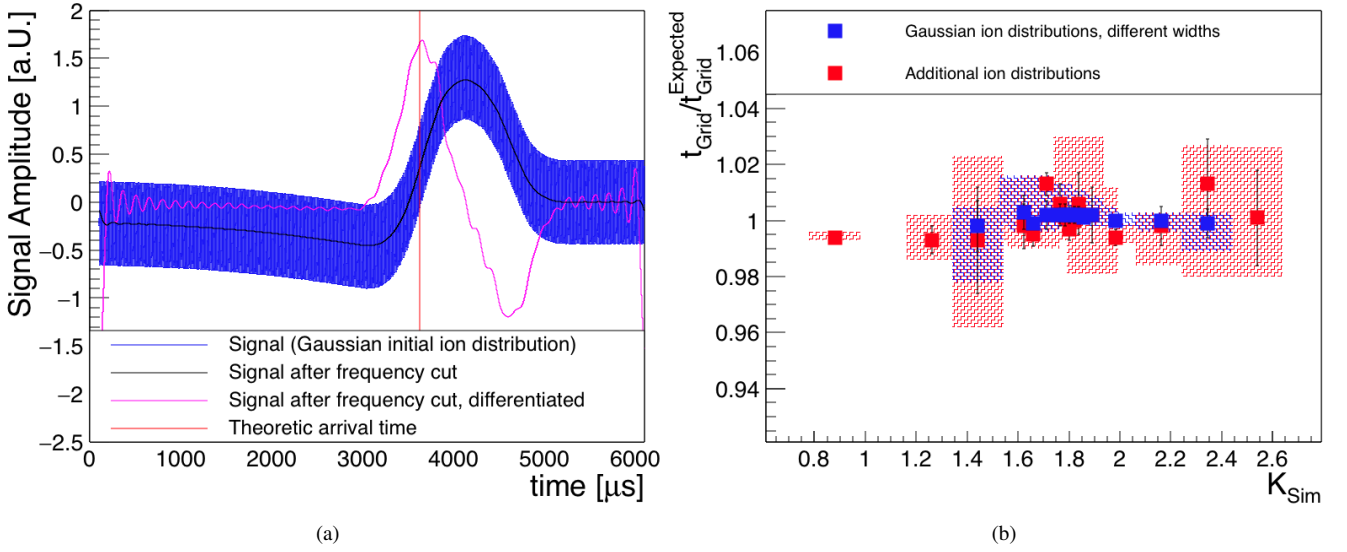


Figure 4: (a) With Garfield the signal induced by ions on the wire-grid is simulated and overlaid with a periodic noise. These modified simulations are analysed with the procedure used for measured signals. Signal simulations, as in Figure (a), are done for varying initial ion distribution and mobilities (K_{Sim}). Different threshold frequencies are used for the frequency cut during the signal analysis procedure. The time at which the ions pass the wire-grid (t_{Grid}) is extracted from these signals and compared to the value expected from the input parameters of the simulation ($t_{\text{Grid}}^{\text{Expected}}$). (b) $t_{\text{Grid}}/t_{\text{Grid}}^{\text{Expected}}$ as function of K_{Sim} . The vertical bands show the full range of different t_{Grid} extracted for different f_{Cut} , while the average (respectively standard deviation) of the corresponding t_{Grid} values is marked by a square (respectively the error bars).

gas amplification in the GEM stack. The distribution is measured using the induced ion signal at the GEM1 bottom electrode. Ions from the electron amplification in GEM3 dominate the signal at our high voltage settings, however, there is a small contribution of ions originating at GEM2. These ions are spread in space, hence t_{GEM} should be defined as the time when half of the ions has crossed GEM1 and entered the drift gap.

3.4. Measurement of the ions entering the drift gap

The signal induced on the GEM1 bottom electrode rises as the ions move towards it, and falls when the ions either cross GEM1 or are collected by the electrode (Fig. 2). The maximum of this signal thus corresponds to the time when the ions reach the level of GEM1 bottom. The voltage settings of the GEM stack are tuned to reach a small width of the ion signal's peak. Ideally t_{GEM} is the time at which the ions pass the GEM1 top electrode, hence an offset due to the width of the GEM foil ($\sim 50 \mu\text{m}$) is introduced using the peak in the GEM1 bottom signal. The time it takes one ion to cross GEM1 can be estimated to be lower than $1 \mu\text{s}$, using conservative values for the mobility and the electric field inside the GEM hole ($K = 1 \text{ cm}^2 \text{ V}^{-1} \text{ s}^{-1}$, $E_{\text{GEM}} = 10 \text{ kV cm}^{-1}$). On the other hand, the field leakage from the GEM1 holes into the drift volume produces a small, local increase of the drift field near the GEM. We therefore ignore these two, competing effects and chose the start-time of the ions' drift time measurement (t_{GEM}) to be the time of the highest amplitude in the GEM1 bottom signal.

4. Results

For a given gas mixture, the induced signals at the GEM1 bottom electrode and at the wire-grid are simultaneously recorded.

These signals are averaged over 2000 or 3000 subsequent events for each field setting. The ions' drift time is extracted as explained in Section 3.1 and 3.4 and the ion mobility $K(E_{\text{Drift}})$ is calculated (Eq. (1)). We apply the commonly used density correction (e.g. [1, 8]) to the gas density at 273.15 K and 1013 mbar to calculate the reduced mobility K_0 using T_{Meas} and P_{Meas} during each measurement.²

$$K_0 = K \cdot \frac{273.15 \text{ K}}{T_{\text{Meas}}} \cdot \frac{P_{\text{Meas}}}{1013 \text{ mbar}} \quad (2)$$

The actual results are shown from Section 4.2 on. In the following we discuss shortly the uncertainties affecting our measurement.

4.1. Estimate of uncertainties in the experiment

4.1.1. Time measurements

The drift time of the ions (t_{Drift} in Eq. (1)) is calculated from t_{GEM} and t_{Grid} . The start time, t_{GEM} , is determined as the time at which the peak in the signal from the GEM1 bottom electrode reaches its most negative amplitude (cf. Sec. 3.4). In Figure 2 t_{GEM} is marked by the first vertical line. A minimum (maximum, respectively) of the oscillations peaking close to (at, respectively) the actual minimum in the signal, will lead to a shift of the measured t_{GEM} . Therefore the uncertainty on t_{GEM} is half an oscillation period, i.e. $\delta(t_{\text{GEM}}) = 20 \mu\text{s}$.

The t_{Grid} measurement is examined with the simulations discussed in Section 3.1. The removal of the oscillations on top of

²The pressure and temperature in our detector is on average $T_{\text{Meas}} \sim 293.5 \text{ K}$ and $P_{\text{Meas}} \sim 966 \text{ mbar}$ with a standard deviation of 1.5 K and 9 mbar, respectively.

the actual signal introduces an uncertainty on t_{Grid} . After applying the frequency cut, oscillations remain in the grid signal and in turn in its derivative. The location of the maxima in the derivative's oscillations influences the found t_{Grid} . We quantified the uncertainty on the t_{Grid} measurement due to this effect with simulations of the wire-grid signal (Sec. 3.1). Figure 4b shows the ratio $t_{\text{Grid}}/t_{\text{Grid}}^{\text{Expected}}$ and the spread of this quantity occurring when f_{Cut} is varied. Based on this test we conclude that the relative error of our method to determine t_{Grid} is not larger than $\pm 2\%$. The error on t_{Grid} is hence $\delta(t_{\text{Grid}}) = 0.02 \cdot t_{\text{Grid}}$.

Gaussian error propagation is used to calculate the error on the full drift time $t_{\text{Drift}} = t_{\text{Grid}} - t_{\text{GEM}}$

$$\begin{aligned}\delta(t_{\text{Drift}}) &= \sqrt{\delta(t_{\text{Grid}})^2 + \delta(t_{\text{GEM}})^2} \\ &= \sqrt{(0.02 \cdot t_{\text{Grid}})^2 + (20 \mu\text{s})^2} \quad .\end{aligned}\quad (3)$$

4.1.2. Set-voltages

The uncertainty on each set voltage is $\delta(U_{\text{Set}}) = 2 \text{ V}$. Therefore the full uncertainty on the voltage difference across the drift gap is

$$\begin{aligned}\delta(\Delta U_{\text{Drift}}) &= \\ \sqrt{\delta(U_{\text{GEM1 Top}})^2 + \delta(U_{\text{Grid}})^2} &= \sqrt{2} \cdot 2 \text{ V} \quad .\end{aligned}\quad (4)$$

This uncertainty is fully correlated among subsequent measurements without changing the voltages in-between. However, the mobility is always measured for different E_{Drift} and therefore different voltage settings.

4.1.3. Drift length

The error on the drift length $\delta(d_{\text{Drift}})$ is a systematic uncertainty, which is fully correlated among all measurements with the same d_{Drift} . The measurement of the spacers used to define the drift length yields an uncertainty of about 0.1 mm (Sec. 2).

4.1.4. Gas conditions

We assume conservative statistical errors of the pressure and temperature of $\delta(P_{\text{Meas}}) = 1 \text{ mbar}$ and $\delta(T_{\text{Meas}}) = 0.5 \text{ K}$, respectively. The flow stability of the employed mass flow meters is 0.1 %. Considering the highest and lowest flow used during all measurements, the largest uncertainty on a mixing ratio is estimated to be lower than 1.7 %. *E.g.*: The uncertainty of a 10 % component of a gas mixture is thus 0.17 %.

4.2. Mobility as function of E_{Drift}

Figure 5 shows the inverse of the reduced mobility K_0 as a function of E_{Drift} for different Ar-CO₂ and Ne-CO₂ mixtures. The drift field (E_{Drift}/N , respectively) ranges from 200 V cm⁻¹ to 1100 V cm⁻¹ (0.84 Td to 4.6 Td, respectively³) while the average gas pressure and temperature is $966 \pm 9 \text{ mbar}$ and $293.5 \pm 1.5 \text{ K}$, respectively. For these values of E_{Drift} , the (reduced) ion mobility of each mixture is found to be constant, which is the

expected behaviour for low electric fields. (For high fields the mobility changes with the electric field with a $K \sim 1/\sqrt{E}$ dependence [28].) An electric field is considered as low, if the energy, gained by an ion from the field, is much smaller than the thermal energy (*cf.* [1]) *i.e.* if

$$\left(\frac{m_1}{m_2} + \frac{m_2}{m_1}\right) eEl \ll kT \quad , \quad (5)$$

where the masses m_1 and m_2 have to be chosen according to the masses of the ion and its collision partner and l is the mean free path between collisions. The mass factor in Equation (5) will be ≥ 2 , considering the masses of the atoms and molecules in the used gas mixtures. The inequality is thus not fulfilled ($l = 100 \text{ nm}$, $E = 1000 \text{ V cm}^{-1}$)⁴ at our gas conditions, however, the energy gained from the field is not much larger than kT . We therefore measure $K(E_{\text{Drift}})$ in a range where the transition from $K \sim \text{const}$ to $K \sim 1/\sqrt{E}$ takes place and the observed constant $K_0^{\text{Mix}}(E_{\text{Drift}})$ are reasonable.

4.3. Blanc's law for Ar- and Ne-CO₂

Since the measured mobilities do not depend on the drift field, a weighted mean of the measurements is calculated, weighting each measurement with its uncertainty. The corresponding error of the weighted mean is calculated and added in quadrature with the systematic uncertainty on the drift length.

No indication for more than one drifting ion species is observed in the data, which fits the expectation that only one type of (CO₂ based cluster) ion drifts in the Ar-CO₂ and the Ne-CO₂ mixtures [25]. Hence Blanc's law [27] can be applied in order to extract the mobility of these ions in pure argon (respectively neon) and pure carbon-dioxide. To this end a fit of the type

$$\frac{1}{K_0^{\text{Mix}}} = a + f_{\text{CO}_2} (b - a) \quad (6)$$

is applied to the data in each panel of Figure 6. The parameter a and b correspond to $1/K_0^{\text{Ar}}$ (respectively $1/K_0^{\text{Ne}}$) and $1/K_0^{\text{CO}_2}$, respectively, while f_{CO_2} is the CO₂ fraction in the mixture. The superscript on the K_0 s indicates the mobility of the drifting ion in the particular gas or mixture. The extrapolated mobility at 100 % CO₂, $K_0^{\text{CO}_2}$, is compatible, within errors, for both argon and neon mixtures (Table 1). This may indicate that in both mixtures the same (cluster) ion species drifts. The results obtained by the presented method are compatible with other measurements [22, 23, 25, 26].

We compare our results in Table 1 to results of ion mobility measurements for different argon-, neon-, nitrogen-, and carbon-dioxide-based (cluster) ions drifting in the respective pure gases [8, 9, 10, 11]. Most of the mobilities included in these reviews are obtained at different E/N , T_{Meas} or P_{Meas} as compared to the gas conditions present during this work. In [30] a reduced mobility of $1.06 \pm 0.02 \text{ cm}^2 \text{ V}^{-1} \text{ s}^{-1}$ is reported for a not identified carbon-dioxide based cluster ion, possible containing hydrogen, measured in CO₂ ($T_{\text{Meas}} = 298 \text{ K}$, $P_{\text{Meas}} =$

³ N is the neutral particle density and $\text{Td} = 1 \times 10^{-17} \text{ V cm}^2$.

⁴ At $P = 1013 \text{ mbar}$ and $T = 273.15 \text{ K}$ the mean free path between collisions is 39.5 nm, 63.2 nm and 125 nm for pure CO₂, Ar and Ne, respectively [29].

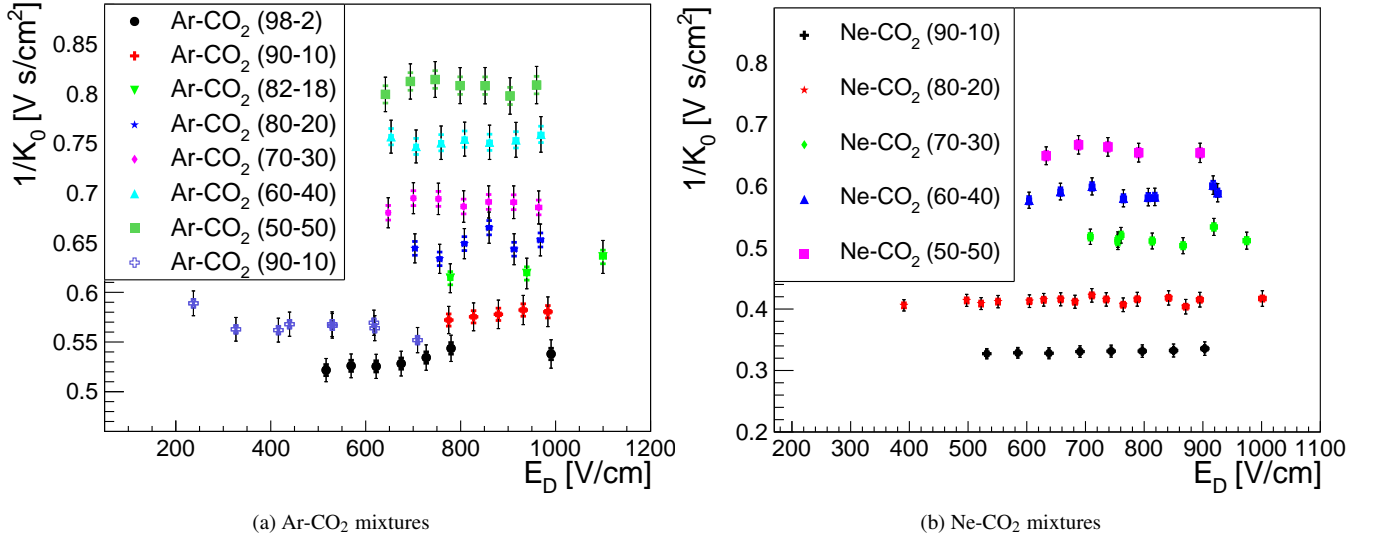


Figure 5: Inverse reduced ion mobility for Ar-CO₂ (Ne-CO₂, respectively) mixtures. All closed (open, respectively) points are measured with a drift length of 21.35 mm (25.31 mm, respectively). The water content in different measurements ranges from 34 ppm to 98 ppm (120 ppm to 180 ppm, respectively) for the Ar-CO₂ (Ne-CO₂, respectively) mixtures. The coloured error-bars represent the error due to the drift length uncertainty, while the black error bar represents the combined uncertainty of all other sources.

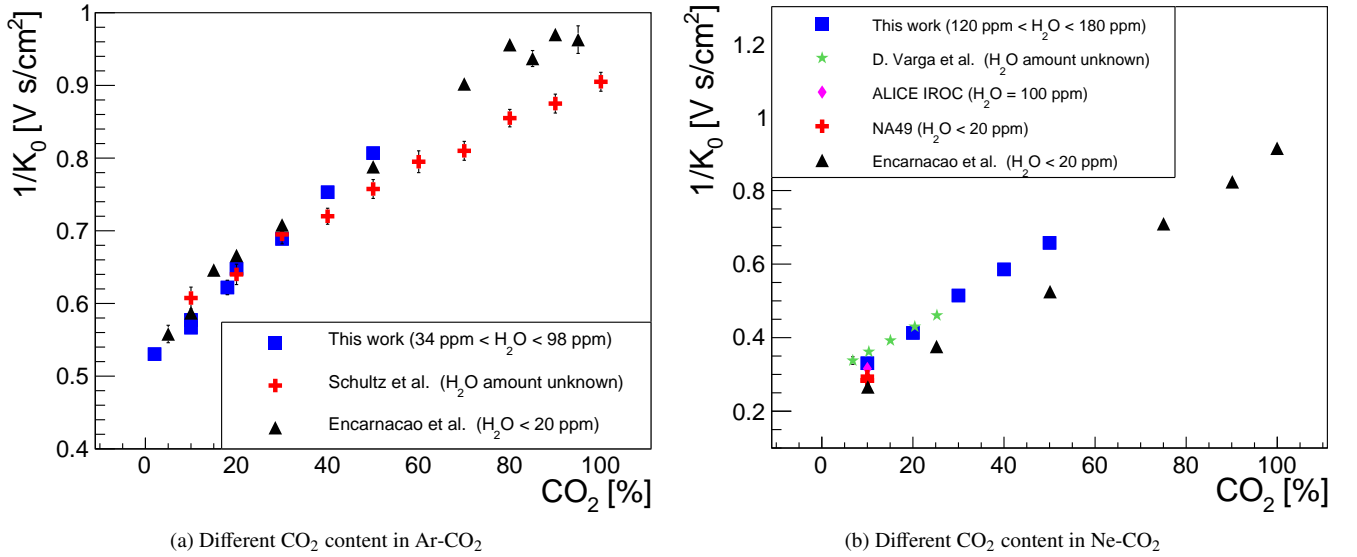


Figure 6: Ion mobilities for the different Ar-CO₂ mixtures (a) (respectively Ne-CO₂ mixtures (b)) result from the corresponding measurements in Figure 5a (respectively 5b). For comparison, results from other groups are shown: *Schultz et al.* cf. [22], *Encarnação et al.* – Ar-CO₂ cf. [23] and Ne-CO₂ cf. [24], *NA41* and *ALICE IROC* cf. [25] and *D. Varga et al.* cf. [26].

	Ar	CO ₂	χ^2/N_{DF}
$K_0 \text{ [cm}^2 \text{ V}^{-1} \text{ s}^{-1}]$	1.94 ± 0.01	1.10 ± 0.01	1.65
	Ne	CO ₂	χ^2/N_{DF}
$K_0 \text{ [cm}^2 \text{ V}^{-1} \text{ s}^{-1}]$	4.06 ± 0.07	1.09 ± 0.01	4.62

Table 1: Fit results of a linear fit according to Equation (6) are shown. The fit has been performed to our data displayed in Figures 6a and 6b. According to Blanc's law [27], the reduced ion mobilities here are the mobilities in pure argon, neon and carbon-dioxide for the ion species drifting in the Ar-CO₂ and Ne-CO₂ mixtures used in the measurements. N_{DF} is the number of the degrees of freedom of the fit.

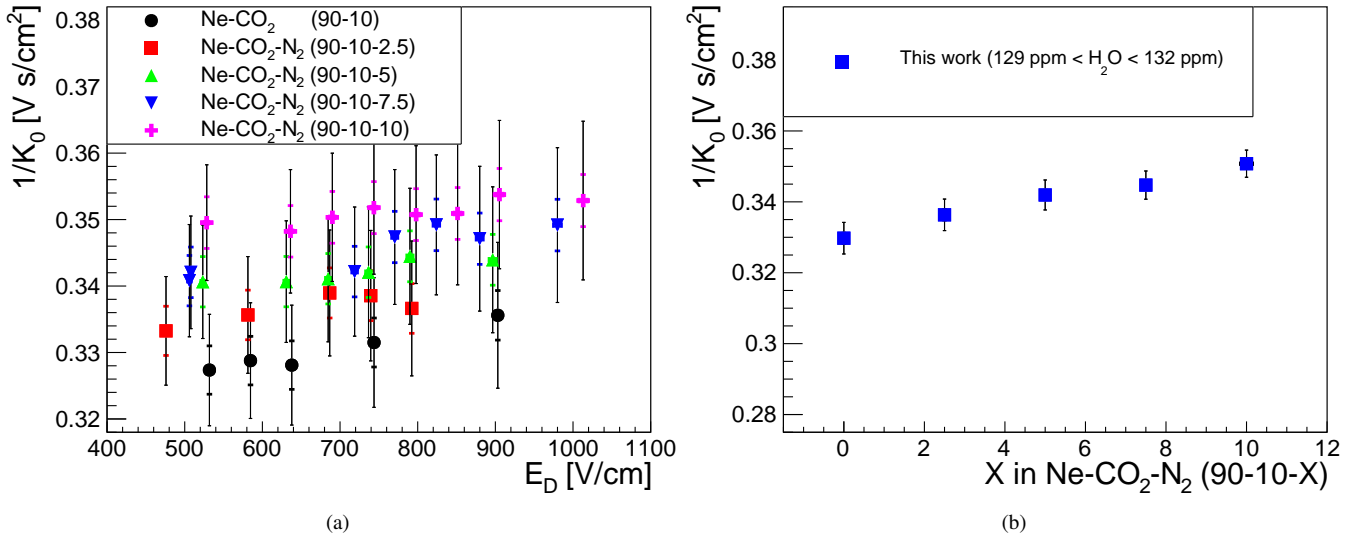


Figure 7: Measurements of $1/K_0$ for different amount of N₂ admixtures to a Ne-CO₂ (90-10) gas mixture. Figure (a) shows one over the reduced mobility for different E_{Drift} for different Ne-CO₂-N₂ mixtures. The ratios (90-10-X) are not meant to be interpreted as % ratios but mixing ratios. The same convention for the error bars as in Figure 5 is used here. The points in (b) correspond to the average of each of these measurement series.

1016 mbar). This value is compatible with our $K_0^{CO_2}$, gained from the Ar-CO₂ and Ne-CO₂ measurements (Table 1). Thus the comparison to the [30] data is a strong indication that the drifting ion species in Ar-CO₂ and Ne-CO₂ is a CO₂ based cluster ion as is suggested for these gas mixtures [25]. A reduced mobility of $\sim 1.1 \text{ cm}^2 \text{ V}^{-1} \text{ s}^{-1}$ for CO₂⁺CO₂ drifting in carbon dioxide is reported in [31, 11] ($T_{Meas} = 300 \text{ K}$, $P_{Meas} = 0.666 \text{ mbar}$). However, it has to be kept in mind that the ion clustering processes can differ for different gas pressure and temperature [30], which makes an extrapolation between measurements at different T_{Meas} and P_{Meas} not significant.

4.4. N₂ in Ne-CO₂ mixtures

The addition of N₂ to the Ne-CO₂ (90-10) mixture is studied in order to determine K_0 of the baseline gas mixture of the upgraded ALICE TPC. Figure 7a shows several $1/K_0^{Ne-CO_2-N_2}$ measurement series for Ne-CO₂ (90-10) and different amounts of nitrogen.

For Figure 7b we average the $1/K_0^{Ne-CO_2-N_2}$ for each Ne-CO₂-N₂ mixture as done for the mixtures discussed in Section 4.3. Adding nitrogen to a Ne-CO₂ (90-10) gas mixture reduces the (reduced) ion mobility of the resulting mixture. The effect is however small, *i.e.* changing from 0 % nitrogen to 5 % nitrogen, results in a reduction of K_0^{Mix} of about 3.3 %.

A fit of Equation (6) to the data with either $1/K_0^{Ne}$ or $1/K_0^{CO_2}$ fixed to the value in Table 1 yields the mobility of the drifting ion species in Ne-CO₂-N₂ in 100 % nitrogen, $K_0^{N_2} = 1.8 \pm 0.2 \text{ cm}^2 \text{ V}^{-1} \text{ s}^{-1}$. The other free parameter – either K_0^{Ne} or $K_0^{CO_2}$ – is about 8 % lower than the reduced mobility listed in Table 1. This discrepancy together with the relatively high uncertainty on $K_0^{N_2}$ could be an indication that the drifting ion species in Ne-CO₂-N₂ differs from the one in Ne-CO₂. Nitrogen has a higher ionisation energy than carbon-dioxide, water or oxygen

but a lower ionisation energy than neon [32]. The charge transfer from Ne ions to CO₂ molecules could perhaps be modified by the presence of N₂ molecules.

The reduced ion mobility of the baseline gas mixture for the future ALICE TPC Ne-CO₂-N₂ (90-10-5) is $2.92 \pm 0.04 \text{ cm}^2 \text{ V}^{-1} \text{ s}^{-1}$, measured at a water content of $130 \pm 1 \text{ ppm}$.

4.5. Traces of H₂O in Ne-CO₂ (90-10) and Ar-CO₂ (90-10)

In order to have similar gas conditions as are present in the ALICE TPC most of our measurements are done with a water content around 100 ppm. To study the effect of traces of H₂O on the (reduced) ion mobility, the water content in Ar-CO₂ (90-10) (Ne-CO₂ (90-10), respectively) has been increased from about 70 ppm to about 1000 ppm (respectively from $\sim 320 \text{ ppm}$ to $\sim 2050 \text{ ppm}$) (Fig. 8). Water is introduced into the gas by inserting a given length of nylon tubing in the supply, since water diffuses through nylon walls.

In Ar-CO₂ (90-10) (Fig. 8a) no strong effect of water admixtures is visible. The points in the figure are a compilation of several measurements, partially with a large time between subsequent measurements. In case of the Ne-CO₂ (90-10) (Fig. 8b), all measurements are done directly after each other in order to minimise other changes in the gas conditions. In this case, a clear decrease of the reduced mobility with increasing water content can be seen.

The weighted mean of each measurement series is again calculated (Fig. 9). For the Ar-CO₂ (90-10) mixture there is a decreasing trend for $K_0^{Mix}(H_2O)$ as the water content is increased from 72 ppm to about 700 ppm. In Ne-CO₂ (90-10) an increase of the water content in the mixture from 365 ppm to 900 ppm leads to a clear reduction of the mobility by 5.8 %. A measurement series with even higher water content (2200 ppm) has been done, indicating that the decrease of mobility with increasing water content is more prominent at lower water content.

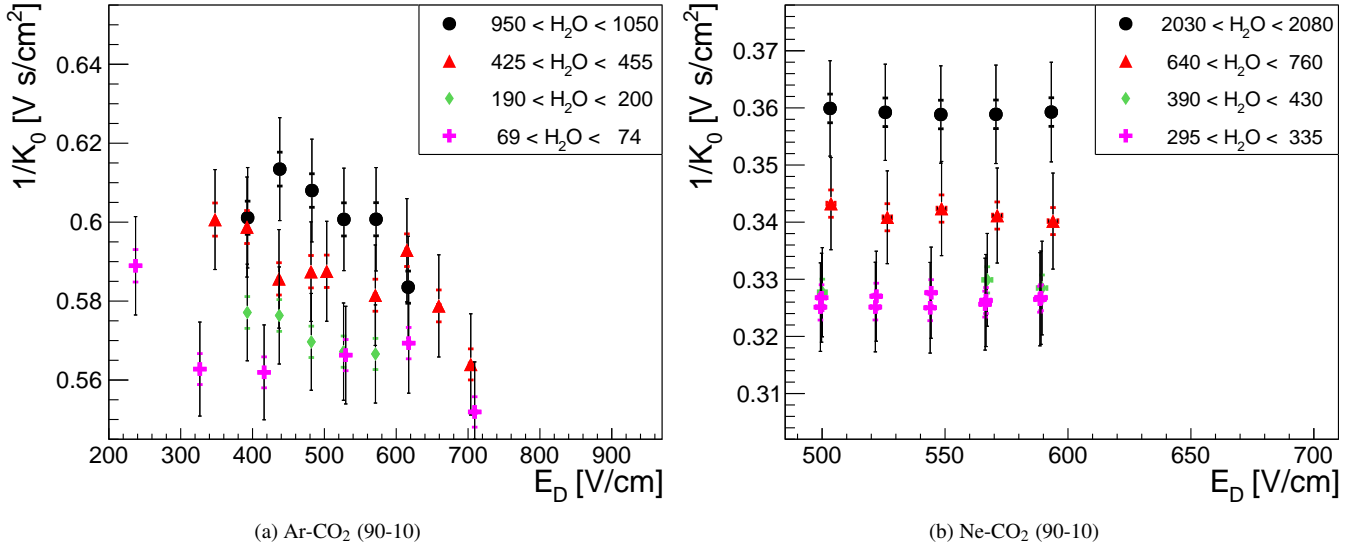


Figure 8: The reduced ion mobility for varying water content in two gas mixtures. The same convention for the error bars as in Figures 5 and 7a applies here.

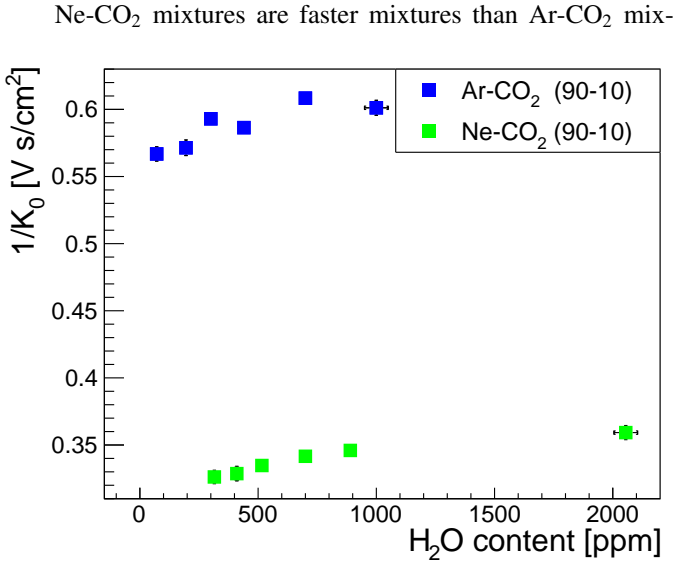


Figure 9: The weighted mean of the data series in Figure 8a (respectively Fig. 8b) showing the change in mobility for varying water content in Ar-CO₂ (90-10) and Ne-CO₂ (90-10), respectively. In addition, results from measurements in Ar-CO₂ (90-10) (Ne-CO₂ (90-10), respectively) at a water content of 700 ± 5 ppm and 300 ± 5 ppm (890 ± 20 ppm and 516 ± 15 ppm, respectively) are included as well in the figure, but are not shown in Figure 8. The horizontal error-bars do not represent an uncertainty, but indicate the range over which the water content is varied.

tures, with respect to the ion velocity. Therefore the impact of the H₂O molecules is more drastic in the Ne-CO₂ case. For varying water content in a gas mixture there are no previous systematic studies in the literature, we are aware of, in order to compare to these measurements. They agree with the assumption that water lowers the ion mobility, as suggested in [25]. In the same paper the authors observe a $\sim 11\%$ lower mobility in Ne-CO₂ (90-10) while comparing measurements done at a water content of less than 20 ppm to a measurement with another

detector using 100 ppm of water. In case the mobility change as a function of H₂O is this drastic at low water content, this change could explain the difference between the Ne-CO₂ results in [24, 25] and this work (Fig. 6b). However, comparing between [23] and our results (Fig. 6a) shows that such an effect is not present in Ar-CO₂ mixtures.

5. Summary

The drift time of ions through a drift gap was measured using two simultaneous recorded signals. The start signal is recorded on the electrode from which the ions initiate their drift. In order to determine the time of arrival of the ions at a wire-grid, defining the end of the drift gap, a novel method was developed. The induced signal over the full ion drift time is recorded. The inflection point of this signal is found to correspond to the ion's arrival time at the grid. From the difference of this two times the mobility is calculated. This has been done for different gas mixtures and for different drift field values in each gas mixture. The effect of water admixtures was examined as well.

The measurements were done for drift fields ranging between 200 V cm^{-1} and 1100 V cm^{-1} at ambient conditions, with a typical water content of about 100 ppm.

Ion mobilities are found to be constant in the explored range of E/P_{Meas} . From fits of Blanc's law to the Ar-CO₂ data we found the reduced mobility of the drifting (cluster) ion in pure argon to be $1.94 \pm 0.01 \text{ cm}^2 \text{ V}^{-1} \text{ s}^{-1}$ and in pure carbon-dioxide to be $1.10 \pm 0.01 \text{ cm}^2 \text{ V}^{-1} \text{ s}^{-1}$. For similar fits to the Ne-CO₂ data we found the reduced mobility of the drifting (cluster) ion to be $4.06 \pm 0.07 \text{ cm}^2 \text{ V}^{-1} \text{ s}^{-1}$ in pure Ne and $1.09 \pm 0.01 \text{ cm}^2 \text{ V}^{-1} \text{ s}^{-1}$ in pure carbon-dioxide. The similarity of both mobilities in CO₂ suggest that the same ion drifts in the argon- as well as the neon-based gas mixture. From a similar analysis of nitrogen admixtures to Ne-CO₂ (90-10) we found a value

of $1.8 \pm 0.2 \text{ cm}^2 \text{ V}^{-1} \text{ s}^{-1}$ for the mobility of the drifting ion in pure nitrogen. It remains to show if the same ion species drifts in Ne-CO₂-N₂ than in Ne-CO₂. Admixtures of N₂ reduced the mobility as compared to pure Ne-CO₂ (90-10) by $\sim 3.3\%$ for an increase of the nitrogen content by 5%. The reduced mobility of the baseline gas mixture of the upgraded ALICE time projection chamber, Ne-CO₂-N₂ (90-10-5) was found to be $2.92 \pm 0.04 \text{ cm}^2 \text{ V}^{-1} \text{ s}^{-1}$. This value was measured with a water content of 130 ppm \pm 1 ppm in the gas mixture.

Furthermore the change of the ion mobility induced by the water content in the gas was examined using Ar-CO₂ (90-10) and Ne-CO₂ (90-10) mixtures. In case of Ar-CO₂ (90-10) a slight decrease of the mobility was observed as the water content is increases from 72 ppm to 700 ppm. While increasing the water content in the Ne-CO₂ (90-10) mixture from 365 ppm to 900 ppm the (reduced) mobility decreased by 5.8%. The effect seemed to level off for a further increase of the H₂O content.

6. Acknowledgements

The authors thank Dr D. Vranic for his contribution to assembling the experimental set-up and for fruitful discussions during the realisation of this work.

References

References

- [1] E. W. McDaniel, E. A. Mason, The mobility and diffusion of ions in gases, 1973.
- [2] J. Alme, Y. Andres, H. Appelshäuser, S. Bablok, N. Bialas, R. Bolgen, U. Bonnes, R. Bramm, P. Braun-Munzinger, R. Campagnolo, et al., The alice tpc, a large 3-dimensional tracking device with fast readout for ultra-high multiplicity events, Nuclear Instruments and Methods in Physics Research Section A: Accelerators, Spectrometers, Detectors and Associated Equipment 622 (1) (2010) 316–367.
- [3] H. Appelsäuser, M. Arslanodok, C. Garabatos, E. Hellbär, M. Ivanov, C. Lippmann, J. Wiechula, K. Schweda, R. Shahoyan, Space-charge distortion measurements and their calibration in the alice tpc, aLICE note in preparation for publication (2017).
- [4] F. Böhmer, M. Ball, S. Dörheim, C. Höppner, B. Ketzer, I. Konorov, S. Neubert, S. Paul, J. Rauch, M. Vandenbroucke, Simulation of space-charge effects in an ungated gem-based tpc, Nuclear Instruments and Methods in Physics Research Section A: Accelerators, Spectrometers, Detectors and Associated Equipment 719 (2013) 101 – 108. arXiv:1209.0482, doi:10.1016/j.nima.2013.04.020. URL <http://www.sciencedirect.com/science/article/pii/S0168900213004166>
- [5] Upgrade of the ALICE Time Projection Chamber, Tech. Rep. CERN-LHCC-2013-020. ALICE-TDR-016, CERN, Geneva (Oct 2013). URL <https://cds.cern.ch/record/1622286>
- [6] T. Krautscheid, Simulation of a pixelized tpc at the ild, Design Studies for the Pixelized Readout of a TPC for the ILD.
- [7] M. Santos, M. Kaja, A. Cortez, R. Veenhof, P. Neves, F. Santos, F. Borges, C. Conde, Experimental ion mobility measurements for the LCTPC collaboration Ar-CF₄ mixtures, Journal of Instrumentation 13 (04) (2018) P04012. URL <http://stacks.iop.org/1748-0221/13/i=04/a=P04012>
- [8] H. W. Ellis, R. Y. Pai, E. W. McDaniel, E. A. Mason, L. A. Viehland, Transport properties of gaseous ions over a wide energy range, Atomic data and nuclear data tables 17 (3) (1976) 177–210. doi:[https://doi.org/10.1016/0092-640X\(76\)90001-2](https://doi.org/10.1016/0092-640X(76)90001-2). URL <http://www.sciencedirect.com/science/article/pii/0092640X76900012>
- [9] H. W. Ellis, E. W. McDaniel, D. L. Albritton, L. A. Viehland, S. L. Lin, E. A. Mason, Transport properties of gaseous ions over a wide energy range. Part II, Atomic Data and Nuclear Data Tables 22 (1978) 179 – 217.
- [10] H. Ellis, M. Thackston, E. McDaniel, E. Mason, Transport properties of gaseous ions over a wide energy range. Part III, Atomic Data and Nuclear Data Tables 31 (1) (1984) 113 – 151. doi:[https://doi.org/10.1016/0092-640X\(84\)90018-4](https://doi.org/10.1016/0092-640X(84)90018-4). URL <http://www.sciencedirect.com/science/article/pii/0092640X84900184>
- [11] L. Viehland, E. Mason, Transport properties of gaseous ions over a wide energy range, iv, Atomic Data and Nuclear Data Tables 60 (1) (1995) 37 – 95. doi:<https://doi.org/10.1006/adnd.1995.1004>. URL <http://www.sciencedirect.com/science/article/pii/S0092640X85710042>
- [12] A. Deisting, C. Garabatos, A. Szabo, D. Vranic, Measurements of ion mobility in argon and neon based gas mixtures, Nuclear Instruments and Methods in Physics Research Section A: Accelerators, Spectrometers, Detectors and Associated Equipment 845 (2017) 215 – 217, proceedings of the Vienna Conference on Instrumentation 2016. doi:<http://doi.org/10.1016/j.nima.2016.06.093>. URL <http://www.sciencedirect.com/science/article/pii/S016890021630660X>
- [13] F. Sauli, GEM: A new concept for electron amplification in gas detectors, Nuclear Instruments and Methods in Physics Research Section A: Accelerators, Spectrometers, Detectors and Associated Equipment 386 (2) (1997) 531–534.
- [14] Bronkhorst, EL-FLOW Select F-201CV, [Online; accessed 08-May-2018]. URL <https://www.bronkhorst.com/products/gas-flow/el-flow-select/f-201cv/>
- [15] First Sensor, CTE / CTU7000 pressure transmitters – datasheet, [Online; accessed 17-May-2018]. URL https://www.first-sensor.com/cms/upload/datasheets/DS_Standard-CTE-CTU7000_E.11507.pdf
- [16] Edgetech Instruments, DewMaster chilled mirror hygrometer, [Online; accessed 03-June-2018]. URL <http://www.edgetechinstruments.com/moisture-humidity/gallery/item/dewmaster-chilled-mirror-hygrometer>
- [17] CAEN, MOD. N471 2 FOLD H.V. POWER SUPPLY, 21st April 1999. [Online; accessed 06-October-2017]. URL <http://www.caen.it/servlet/checkCaenManualFile?Id=5301>
- [18] CAEN, MOD. N 470 4 CHANNEL PROGRAMMABLE H.V. POWER SUPPLY, 2002. [Online; accessed 07-June-2017]. URL www.caen.it/servlet/checkCaenManualFile?Id=5240
- [19] A. ORTEC, Model 142ih preamplifier operating and service manual, 2013. [Online; accessed 06-October-2017]. URL <http://www.ortec-online.com/-/media/ametektortec/manuals/142ih-mnl.pdf>
- [20] S. Ramo, Currents induced by electron motion, Proc. Ire 27 (9) (1939) 584–585.
- [21] Veenhof, Rob, Garfield-simulation of gaseous detectors, Cern Program Library W 5050 (1984) 2001.
- [22] G. Schultz, G. Charpak, F. Sauli, Mobilities of positive ions in some gas mixtures used in proportional and drift chambers, Revue de Physique Appliquée 12 (1) (1977) 67–70.
- [23] P. Encarnação, A. Cortez, M. Pinto, P. Neves, A. Trindade, J. Escada, F. Santos, F. Borges, J. Barata, C. Conde, Experimental ion mobility measurements in Ar-CO₂ mixtures, Journal of Instrumentation 10 (01) (2015) P01010.
- [24] P. Encarnação, A. Cortez, R. Veenhof, P. Neves, F. Santos, A. Trindade, F. Borges, C. Conde, Experimental ion mobility measurements in Ne-CO₂ and CO₂-N₂ mixtures, Journal of Instrumentation 11 (05) (2016) P05005. URL <http://stacks.iop.org/1748-0221/11/i=05/a=P05005>
- [25] Y. Kalkan, M. Arslanodok, A. Cortez, Y. Kaya, İ. Tapan, R. Veenhof, Cluster ions in gas-based detectors, Journal of Instrumentation 10 (07) (2015) P07004.
- [26] D. Varga, Ion mobility: preliminary results, talk at the RD51 mini week, June 2014.

- URL https://indico.cern.ch/event/323839/contributions/751953/attachments/627122/862953/mobility_ArNe.pdf
- [27] M. A. Blanc, Mobilité des ions, *J. Phys. Theor. Appl.* 7 (1908) 825 – 839.
 - [28] W. Blum, W. Riegler, L. Rolandi, Particle detection with drift chambers, Springer Science & Business Media, 2008.
 - [29] K. Jousten (Ed.), *Wutz Handbuch Vakuumtechnik*, no. 7, Vieweg Verlag Braunschweig/Wiesbaden.
 - [30] H. W. Ellis, R. Y. Pai, I. R. Gatland, E. W. McDaniel, R. Wernlund, M. J. Cohen, Ion identity and transport properties in CO₂ over a wide pressure range, *The Journal of Chemical Physics* 64 (10) (1976) 3935–3941. doi : 10.1063/1.432024.
 - [31] Coxon, P. A., Moruzzi, J. L., Positive ion mobilities in carbon dioxide, *J. Phys. Colloques* 40 (C7) (1979) C7–117–C7–118. doi : 10.1051/jphyscol:1979758.
URL <https://doi.org/10.1051/jphyscol:1979758>
 - [32] S. Lias, Ionization Energy Evaluation, NIST Chemistry WebBook, NIST Standard Reference Database (69), retrieved October 29, 2017.